Group-theoretical and resonating Hartree-Fock studies for spin fluctuations in two-dimensional Hubbard model on triangular lattice

Fumikazu Satoh,[1] Masa-aki Ozaki,[2] Takaaki Maruyama,[1] and Norikazu Tomita[1]
[1]*Department of Physics, Yamagata University, 1-4-12 Kojirakawa, Yamagata, 990-8560, Japan*
[2]*Uji, Kyoto, 611-0002, Japan*
(Received 3 October 2011; published 7 December 2011)

Magnetic structures of the two-dimensional Hubbard model on a uniform triangular lattice are investigated from the viewpoint of quantum fluctuations. First, possible spin density wave (SDW) solutions in the unrestricted Hartree-Fock approximation are group theoretically classified for the ordering vectors of $\mathbf{Q}_1 = (\mathbf{G}_a + \mathbf{G}_b)/4$, $\mathbf{Q}_2 = C_3^+\mathbf{Q}_1$, and $\mathbf{Q}_3 = C_3^-\mathbf{Q}_1$. Then, to include the electron correlation effects efficiently, we apply the resonating Hartree-Fock method. It is shown that the spin fluctuations in the metallic ground state at $U/t \sim 4.5$ are reasonably described as hybridization of two different SDW states obtained by the group theoretical classification and their low-energy excited states. These fluctuations make the long-range magnetic order significantly reduced in the correlated ground state.

DOI: 10.1103/PhysRevB.84.245101 PACS number(s): 71.10.Fd, 75.10.Jm

I. INTRODUCTION

Electron correlation effects in geometrically frustrated systems have been attracting much attention in condensed-matter physics. In fact, a lot of experiments, especially for κ-type BEDT-TTF compounds, have clarified that these systems show a variety of interesting and nontrivial ground states, such as superconductivity, noncolinear 120° antiferromagnetism (AF), and a nonmagnetic Mott-type insulating state.[1–4] This variety of ground states indicates inherent multistability of the system and the ground state can be easily changed by small changes in material parameters such as a lattice constant. Such multistability is an important factor in applying these materials to technology. On the other hand, quantum fluctuations inevitably become very large in such a system with multistability, and they make it difficult to theoretically investigate detailed electronic structures beyond the mean-field and perturbative approaches.[5–7] So far, some sophisticated numerical methods, such as the matrix-product-states variational approach (and its derivatives), the path-integral renormalization group (PIRG) method, and variational and quantum Monte Carlo calculations, have been applied for a Heisenberg or Hubbard model on a triangular lattice,[8–12] and they have concluded that the ground state has 120° AF ordering in the Heisenberg limit or strong interaction regime while it is nonmagnetic metal in the weak interaction regime. PIRG also predicted the nonmagnetic insulating state called spin liquid in the intermediate interaction regimes.[9,10] In these numerical researches, they calculated correlation functions to determine the electronic structures of the ground states. In general, however, it is quite difficult to visualize the detailed spin structures and, therefore, to show how the long-range order (LRO) is lost in the so-called nonmagnetic ground states. In the strongly correlated and geometrically frustrated systems, the nonmagnetic state would not be a simple paramagnetism but large quantum fluctuations would eliminate the magnetic LRO. Such detailed information on the magnetic structures would be important not only for fundamental physics but also for technological applications of these frustrated materials.

In this research, we visualize the magnetic quantum fluctuations by superposition of nonorthogonal Slater determinants and explicitly show how long-range spin correlation is lost in the metallic ground state. For systematic understanding of the quantum fluctuations, we first classify the possible spin density wave (SDW) solutions in the unrestricted Hartree-Fock (UHF) approximation from the group theoretical point of view. To clarify quantum fluctuations which reduce or eliminate the LRO, a resonating HF method is applied. It is shown that the quantum fluctuations in the correlated ground state are described mainly by hybridization of two different SDWs and their low-energy excited states. We also show that the character of quantum fluctuations changes when the strength of the on-site Coulomb interaction is changed, though the system stays metallic.

This paper is organized as follows. In Sec. II, we introduce our model and methods. Then, results and discussion are given in Sec. III. Finally, a brief summary is given in Sec. IV.

II. MODEL AND METHOD

In this paper, we consider a two-dimensional (2D) Hubbard model on a uniform triangular lattice. Its Hamiltonian is given by

$$H = -t \sum_{\langle i,j\rangle\sigma} (a^\dagger_{i,\sigma} a_{j,\sigma} + a^\dagger_{j,\sigma} a_{i,\sigma}) + U \sum_{i}^{N} n_{i,\uparrow} n_{i,\downarrow}, \quad (1)$$

where t, U, and N represent a nearest-neighbor hopping, an on-site Coulomb repulsion, and system size, respectively. In the following, we consider a half-filled case and impose a periodic boundary condition. To investigate the electronic structures and quantum fluctuations, we apply a resonating HF method,[13] in which a many-body wave function is constructed by superposition of nonorthogonal Slater determinants, such as

$$|\Psi\rangle = \sum_{n=1}^{N_S} C_n \sum_{G} P^G |\phi_n\rangle. \quad (2)$$

Here N_S represents the number of generating Slater determinants. P^G denotes symmetry projections working on the generating Slater determinants to recover the original

symmetry of the system, as we superpose symmetry-broken Slater determinants to incorporate the electron correlation effects efficiently. Specifically, we employ the general spin orbital (GSO) for the Slater determinants to describe an axial-type SDW (ASDW), plane-type SDW (PSDW), and 3D cubic-type SDW (CSDW). The GSO is an extended molecular orbital and is characterized by the following unitary transformation of the field operators as

$$(c_1,\ldots,c_N,c_{N+1},\ldots,c_{2N}) = (a_{1\uparrow},\ldots,a_{N\uparrow},a_{1\downarrow},\ldots,a_{N\downarrow}) \times \begin{pmatrix} U^{\uparrow\uparrow} & U^{\uparrow\downarrow} \\ U^{\downarrow\uparrow} & U^{\downarrow\downarrow} \end{pmatrix}. \quad (3)$$

Restricted HF orbitals correspond to $U^{\uparrow\downarrow} = U^{\downarrow\uparrow} = 0$ and $U^{\uparrow\uparrow} = U^{\downarrow\downarrow}$, while different orbitals for different spins (DODS) correspond to $U^{\uparrow\downarrow} = U^{\downarrow\uparrow} = 0$ and $U^{\uparrow\uparrow} \neq U^{\downarrow\downarrow}$. The GSO allows nonzero off-diagonal terms, that is, $(U^{\uparrow\downarrow})^\dagger = U^{\downarrow\uparrow} \neq 0$. In this method, orbitals of all the Slater determinants, as well as their superposition coefficients, are simultaneously optimized. The orbital optimization corresponds to finding N_S unitary matrices of $2N$ dimensions, as in Eq. (3), which give the lowest energy expectation value for the Hamiltonian. There is no such restriction as a negative sign problem in a quantum Monte Carlo method or a dimension problem in a density matrix renormalization group method. So far, we have demonstrated that the resonating HF method explains the correlation energies comparable to the variational Monte Carlo or quantum Monte Calro simulations.[14] In addition, we can directly obtain information on quantum fluctuations by analyzing the structures of generating Slater determinants.[15] For an efficient orbital optimization and analysis, it is important to know the UHF ground and excited states. It would be reasonable to employ such UHF ground and low-energy excited states as initial Slater determinants of the resonating Hartree-Fock wave function, though the orbital optimization might make the final Slater determinants somewhat different from these initial guesses. Practical applications are given in Sec. III. We can also refer the UHF states to describe the electronic structures and quantum fluctuations of the system. Thus, it is important to classify such UHF solutions systematically, before applying the resonating HF method.

A group theory is a powerful tool to classify symmetry-broken solutions in the HF or HF-Bogoliubov equations.[16–18] In general, Hamiltonian has a symmetry of

$$G_0 = P \times S \times R, \quad (4)$$

where P, S, and R denote space, spin rotation, and time-reversal groups, respectively. We should note that a uniform triangular lattice has a $\mathbf{D}_6 L(\mathbf{t}_a,\mathbf{t}_b)$ space group, where $L(\mathbf{t}_a,\mathbf{t}_b)$ denotes the translation symmetry group for the unit translation vectors $\mathbf{t}_a$ and $\mathbf{t}_b$ of the lattice shown in Fig. 1(1). Classification of UHF solutions corresponds to the classification of representation spaces spanned by the order parameter vectors, according to the equivalent branching lemma.[19,20] After the Fourier transformation, such as

$$a^\dagger_{i,\sigma} = \frac{1}{\sqrt{N}} \sum_{\mathbf{k}} a^\dagger_{\mathbf{k}\sigma} e^{i\mathbf{k}\cdot\mathbf{r}_i}, \quad (5)$$

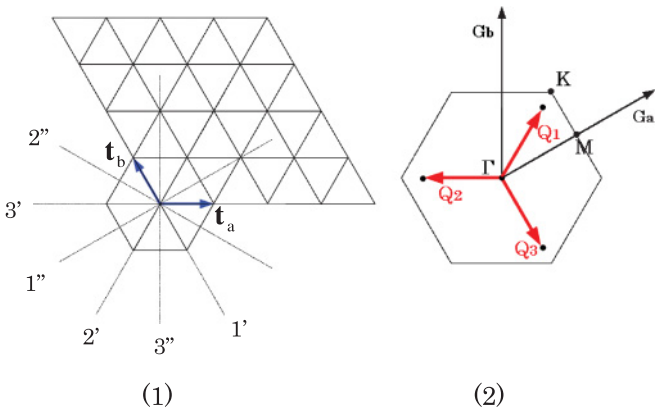

FIG. 1. (Color online) A uniform triangular lattice in real space (1) and reciprocal vector space (2). In (1), the dotted lines represent the symmetry lines about spatial and spin rotations.

and applying the HF approximation, the Hamiltonian takes the form

$$H_{\rm HF} = \sum_{\mathbf{k}} \epsilon(\mathbf{k}) \tilde{a}^\dagger_{\mathbf{k}} \tilde{a}_{\mathbf{k}} + \sum_{\mathbf{q}} \sum_{i=0,x,y,z} Z^i_{\mathbf{q}} \sum_{\mathbf{k}} \tilde{a}^\dagger_{\mathbf{k}+\mathbf{q}/2} \sigma_i \tilde{a}_{\mathbf{k}-\mathbf{q}/2}, \quad (6)$$

where $\tilde{a}^\dagger_{\mathbf{k}}$ is a spinor representation of the field operators, such as

$$\tilde{a}^\dagger_{\mathbf{k}} = (a^\dagger_{\mathbf{k}\uparrow}, a^\dagger_{\mathbf{k}\downarrow}). \quad (7)$$

Here σ_0 is a 2×2 identity matrix and σ_i $(i = x,y,z)$ are Pauli matrices. In the following, for a systematic notation, we use $i = 1, 2$, and 3 for x, y, and z components of spin, respectively. $Z^i_{\mathbf{q}}$ is a self-consistent field defined by

$$Z^0_{\mathbf{q}} = \frac{U}{2}\rho_0(\mathbf{q}), \qquad Z^i_{\mathbf{q}} = -\frac{U}{2}\rho_i(\mathbf{q}), \qquad (i = 1,2,3), \quad (8)$$

where

$$\rho_i(\mathbf{q}) = \frac{1}{N} \sum_{\mathbf{k}} \langle \tilde{a}^\dagger_{\mathbf{k}-\mathbf{q}/2} \sigma_i \tilde{a}_{\mathbf{k}+\mathbf{q}/2} \rangle. \quad (9)$$

Here we focus on the SDW solutions to understand the magnetic structures of the system. In the present research, we employ the GSO to describe the coplanar PSDW and 3D CSDW states, as well as the collinear ASDW state. As a result, $\rho_i(\mathbf{q})$ can be finite even when $i = 1$ and 2. As seen from Eq. (6), the order parameter space of $H_{\rm HF}$ is spanned by

$$l_{i,\mathbf{q}} \equiv \sum_{\mathbf{k}} \tilde{a}^\dagger_{\mathbf{k}+\mathbf{q}/2} \sigma_i \tilde{a}_{\mathbf{k}-\mathbf{q}/2}. \quad (10)$$

We can construct Hermitian bases by

$$\Lambda_{i,\mathbf{q},1} = \frac{1}{2}(l_{i,\mathbf{q}} + l_{i,-\mathbf{q}}), \qquad \Lambda_{i,\mathbf{q},2} = \frac{i}{2}(l_{i,\mathbf{q}} - l_{i,-\mathbf{q}}), \quad (11)$$

where we use the relation $l^\dagger_{i,\mathbf{q}} = l_{i,-\mathbf{q}}$. Now the problem is reduced to classifying the order parameter spaces Γ, which are spanned by $\{\Lambda_{i,\mathbf{q},1}, \Lambda_{i,\mathbf{q},2}\}$ and are also the representation spaces of the symmetry group G_0. So far, Ikawa and Ozaki have classified the UHF solutions for $K(\mathbf{q} = (\mathbf{G}_a + \mathbf{G}_b)/3)$ and $M(\mathbf{q} = \mathbf{G}_a/2)$ points,[21] where $\mathbf{G}_a = (2\pi, 2\pi/\sqrt{3})$ and $\mathbf{G}_b = (0, 4\pi/\sqrt{3})$ are reciprocal lattice vectors shown in Fig. 1(2)

(the lattice constant is set as unity). The famous 120° AF state is classified as a PSDW in K point. In this research, we focus on the UHF SDW solutions with the ordering vectors $\mathbf{Q}_1 = \frac{1}{4}(\mathbf{G}_a + \mathbf{G}_b)$ and its $C_3^{\pm}$-rotated vectors $\mathbf{Q}_2$ and $\mathbf{Q}_3$. As shown below, some UHF solutions classified by these ordering vectors play important roles in understanding complicated magnetic structures of the system. By applying the elements of $\mathbf{D}_6$ group, we can see that these $\mathbf{Q}_1$, $\mathbf{Q}_2$, and $\mathbf{Q}_3$ make up a set of fundamental vectors,

$$\begin{aligned}
\mathbf{Q}_1 &= \tfrac{1}{4}(\mathbf{G}_a + \mathbf{G}_b),\\
C_3^+\mathbf{Q}_1 &= \tfrac{1}{4}(-2\mathbf{G}_a + \mathbf{G}_b) \equiv \mathbf{Q}_2,\\
C_3^-\mathbf{Q}_1 &= \tfrac{1}{4}(\mathbf{G}_a - 2\mathbf{G}_b) \equiv \mathbf{Q}_3,\\
C_6^+\mathbf{Q}_1 &= -\mathbf{Q}_3, \quad C_6^-\mathbf{Q}_1 = -\mathbf{Q}_2,\\
C_2\mathbf{Q}_1 &= -\mathbf{Q}_1, \quad C_{21'}\mathbf{Q}_1 = \mathbf{Q}_2,\\
C_{22'}\mathbf{Q}_1 &= \mathbf{Q}_1, \quad C_{23'}\mathbf{Q}_1 = \mathbf{Q}_3,\\
C_{21''}\mathbf{Q}_1 &= -\mathbf{Q}_2, \quad C_{22''}\mathbf{Q}_1 = -\mathbf{Q}_1,\\
C_{23''}\mathbf{Q}_1 &= -\mathbf{Q}_3.
\end{aligned} \tag{12}$$

Here C_n represents $2\pi/n$ rotation around the z axis (perpendicular to the plane), while C_{2p} represents π rotation around the p axis shown in Fig. 1(1). The indices + and − represent the counterclockwise and clockwise directions of the rotation, respectively. As a result, we should classify the order parameter spaces Γ spanned by 18 bases, $\Lambda_{i,m,1}$ and $\Lambda_{i,m,2}$, where i is an index for three components of spin and m is an index for $\mathbf{Q}_m (m = 1,2,3)$. For this purpose, we should note the following relations for the symmetry operations,

(i) From Eqs. (5), (10), and (11), the translation operator $T(\mathbf{n})$ transforms the bases of the order parameter spaces, as

$$T(\mathbf{n})(\Lambda_{i,m,1},\Lambda_{i,m,2}) = (\Lambda_{i,m,1},\Lambda_{i,m,2}) \times \begin{pmatrix} \cos \mathbf{Q}_m\mathbf{n} & \sin \mathbf{Q}_m\mathbf{n} \\ -\sin \mathbf{Q}_m\mathbf{n} & \cos \mathbf{Q}_m\mathbf{n} \end{pmatrix}. \tag{13}$$

(ii) Spin rotation around the $\mathbf{e}$ axis is explicitly given by

$$u(\mathbf{e},\theta)\Lambda_{i,m,1(2)} = \sum_j \mathbf{R}(\mathbf{e},\theta)_{ji}\Lambda_{j,m,1(2)}, \tag{14}$$

where $\mathbf{e} = (n_1,n_2,n_3)$ and $\mathbf{R}(\mathbf{e},\theta)$ is a 3D matrix given by

$$\begin{pmatrix} \cos\theta + (1-\cos\theta)n_1^2 & (1-\cos\theta)n_1n_2 - n_3\sin\theta & (1-\cos\theta)n_1n_3 + n_2\sin\theta \\ 1-\cos\theta)n_1n_2 + n_3\sin\theta & \cos\theta + (1-\cos\theta)n_2^2 & (1-\cos\theta)n_2n_3 - n_1\sin\theta \\ (1-\cos\theta)n_1n_3 - n_2\sin\theta & (1-\cos\theta)n_2n_3 + n_1\sin\theta & \cos\theta + (1-\cos\theta)n_3^2 \end{pmatrix}. \tag{15}$$

In the following, the spin rotation by $2\pi/n$ around the p axis is represented by u_{np}. p can be the x,y,z axes, the $1',1'',2',2'',3',3''$ axes in Fig. 1(1). Spin rotations around $a(y = x)$ and $b(y = -x)$ axes are also used and they are represented by

$$u_{2a} = u_{2x}u_{4z}^-, \quad u_{2b} = u_{2x}u_{4z}^+. \tag{16}$$

(iii) By applying the time-reversal operator t, we obtain

$$\begin{aligned}
t\cdot a_{\mathbf{k}\uparrow}^\dagger &= -a_{-\mathbf{k}\downarrow}^\dagger, \quad t\cdot a_{\mathbf{k}\uparrow} = -a_{-\mathbf{k}\downarrow},\\
t\cdot a_{\mathbf{k}\downarrow}^\dagger &= a_{-\mathbf{k}\uparrow}^\dagger, \quad t\cdot a_{\mathbf{k}\downarrow} = a_{-\mathbf{k}\uparrow},
\end{aligned} \tag{17}$$

which result in

$$t\cdot\Lambda_{i,m,1(2)} = -\Lambda_{i,m,1(2)}. \tag{18}$$

(iv) From Eq. (12), we obtain

$$\begin{aligned}
C_6^+\Lambda_{i,1,1} &= \Lambda_{i,3,1}, \quad C_6^+\Lambda_{i,1,2} = -\Lambda_{i,3,2},\\
C_6^+\Lambda_{i,2,1} &= \Lambda_{i,1,1}, \quad C_6^+\Lambda_{i,2,2} = -\Lambda_{i,1,2},\\
C_6^+\Lambda_{i,3,1} &= \Lambda_{i,2,1}, \quad C_6^+\Lambda_{i,3,2} = -\Lambda_{i,2,2},
\end{aligned} \tag{19}$$

where we should note that $\mathbf{Q}_1$, $\mathbf{Q}_2$, and $\mathbf{Q}_3$ go to $-\mathbf{Q}_3$, $-\mathbf{Q}_1$, and $-\mathbf{Q}_2$ by C_6^+ rotation, respectively. We should also note, from Eq. (12) or geometrical relation shown in Fig. 1(2),

$$\begin{aligned}
C_{21'}\Lambda_{i,1,1(2)} &= \Lambda_{i,2,1(2)}, \quad C_{21'}\Lambda_{i,2,1(2)} = \Lambda_{i,1,1(2)},\\
C_{21'}\Lambda_{i,3,1(2)} &= \Lambda_{i,3,1(2)}.
\end{aligned} \tag{20}$$

We obtain similar relations for π rotations around other axes $(1'',2',2'',..)$, though we do not show them here.

III. RESULTS AND DISCUSSION

A. UHF solutions with SDW ordering

Possible UHF solutions are summarized in Tables I and II, where the bases of the order parameter spaces and invariance groups are shown, respectively. These solutions are obtained according to the equivalent branching lemma, namely, finding the 1D bases of the order parameter spaces.[19,20] Here we show some examples of how to find the UHF solutions and explain the spin structures of the SDW solutions.

TABLE I. Bases of the order parameter spaces for the classified SDW solutions.

SDW	Basis of Γ
ASDW_1	$\Lambda_{3,1,1}$
ASDW_2	$\Lambda_{3,1,1} - \Lambda_{3,1,2}$
ASDW_3	$\Lambda_{3,1,1} + \Lambda_{3,2,1}$
ASDW_4	$\Lambda_{3,1,1} - \Lambda_{3,1,2} + \Lambda_{3,2,1} - \Lambda_{3,2,2}$
ASDW_5	$\Lambda_{3,1,1} + \Lambda_{3,2,1} + \Lambda_{3,3,1}$
ASDW_6	$\Lambda_{3,1,2} + \Lambda_{3,2,2} + \Lambda_{3,3,2}$
PSDW_1	$\Lambda_{1,1,1} - \Lambda_{2,1,2}$
PSDW_2	$\Lambda_{1,1,1} - \Lambda_{2,2,2}$
PSDW_3	$\Lambda_{2,1,1} - \frac{\sqrt{3}}{2}\Lambda_{1,2,1} - \frac{1}{2}\Lambda_{2,2,1} + \frac{\sqrt{3}}{2}\Lambda_{1,3,1} - \frac{1}{2}\Lambda_{2,3,1}$
PSDW_4	$\Lambda_{2,1,2} - \frac{\sqrt{3}}{2}\Lambda_{1,2,2} - \frac{1}{2}\Lambda_{2,2,2} + \frac{\sqrt{3}}{2}\Lambda_{1,3,2} - \frac{1}{2}\Lambda_{2,3,2}$
CSDW_1	$\Lambda_{1,1,1} + \Lambda_{2,2,1} + \Lambda_{3,3,1}$
CSDW_2	$\Lambda_{1,1,2} + \Lambda_{2,2,2} + \Lambda_{3,3,2}$

1. $ASDW_1 \sim ASDW_6$

These SDW solutions have a spin rotation symmetry around a certain axis. For convenience, we choose the z axis for this symmetry axis. First, let us take $\Lambda_{3,1,1}$ as a basis of the order parameter space Γ_1. Obviously, this is one of the simplest 1D bases. From Eq. (13), we obtain

$$\begin{aligned} &T(2\mathbf{t}_a)\Lambda_{3,1,1} = -\Lambda_{3,1,1}, \quad T(2\mathbf{t}_b)\Lambda_{3,1,1} = -\Lambda_{3,1,1}, \\ &T(\mathbf{t}_a - \mathbf{t}_b)\Lambda_{3,1,1} = \Lambda_{3,1,1}. \end{aligned} \tag{21}$$

With Eqs. (12) and (21), we can see that this basis is invariant for $\mathbf{D}_2 L(\mathbf{t}_a - \mathbf{t}_b, 2\mathbf{t}_a + 2\mathbf{t}_b)$. Here the $\mathbf{D}_2$ symmetry group comes from C_2 and $C_{22'}$ (or $C_{22''}$) rotation symmetries of $\Lambda_{3,1,1}$. In addition, from Eqs. (14) and (15), this basis is antisymmetric for the spin rotations by π around the x and y axes, while it is symmetric for the spin rotations around the z axis, such as

$$\begin{aligned} u_{2x}\Lambda_{3,1,1} &\equiv u(\mathbf{e}_x,\pi)\Lambda_{3,1,1} = -\Lambda_{3,1,1}, \\ u_{2y}\Lambda_{3,1,1} &\equiv u(\mathbf{e}_y,\pi)\Lambda_{3,1,1} = -\Lambda_{3,1,1}, \\ u(\mathbf{e}_z,\theta)\Lambda_{3,1,1} &= \Lambda_{3,1,1}. \end{aligned} \tag{22}$$

With Eq. (18), we can see that the invariance group of Γ_1 is

$$\begin{aligned} G(\Gamma_1) = \mathbf{D}_2 L(\mathbf{t}_a - \mathbf{t}_b, 2\mathbf{t}_a + 2\mathbf{t}_b)[E + T(2\mathbf{t}_a)u_{2x} \\ + T(2\mathbf{t}_b)u_{2y}]A(\mathbf{e}_z)M(\mathbf{e}_y), \end{aligned} \tag{23}$$

where $A(\mathbf{n}) = \{u(\mathbf{n},\theta), 0 \leqslant \theta \leqslant 2\pi\}$ and $M(\mathbf{n}) = \{E, tu(\mathbf{n},\pi)\}$. We should note that we can express this invariance group with different combinations of operators but, of course, they are equivalent to each other. This subgroup represents a collinear axial SDW (ASDW) solution and is denoted by $ASDW_1$ in Tables I and II. The spin structure of this state is shown in Fig. 2(1). We also obtain the geometrically equivalent ASDW solutions for $\Lambda_{3,2,1}$ and $\Lambda_{3,3,1}$.

Next, we take $\Lambda_{3,1,1} - \Lambda_{3,1,2}$ as a basis of the order parameter space Γ_2. Applying the translation and spin rotation operators gives the same relations as Eqs. (21) and (22), respectively. On the other hand, this basis does not have a spatial rotation symmetry around the z axis. For example, $\Lambda_{3,1,2}$ is antisymmetric for C_2 rotation, as seen from Eq. (12). Instead, it satisfies

$$C_{22'}(\Lambda_{3,1,1} - \Lambda_{3,1,2}) = \Lambda_{3,1,1} - \Lambda_{3,1,2}. \tag{24}$$

Thus, we obtain the invariance group of Γ_2 as

$$\begin{aligned} G(\Gamma_2) = \mathbf{C}_2' L(\mathbf{t}_a - \mathbf{t}_b, 2\mathbf{t}_a + 2\mathbf{t}_b)[E + T(2\mathbf{t}_a)u_{2x} + T(2\mathbf{t}_b)u_{2y} \\ + T(\mathbf{t}_a)C_2 + T(\mathbf{t}_b)C_2]A(\mathbf{e}_z)M(\mathbf{e}_y), \end{aligned} \tag{25}$$

where $\mathbf{C}_2' = \{E, C_{22'}\}$ and we used the following relations obtained from Eqs. (12) and (13),

$$\begin{aligned} C_2\Lambda_{3,1,1} &= \Lambda_{3,1,1}, \quad C_2\Lambda_{3,1,2} = -\Lambda_{3,1,2}, \\ T(\mathbf{t}_a)\Lambda_{3,1,1} &= T(\mathbf{t}_b)\Lambda_{3,1,1} = -\Lambda_{3,1,2}, \\ T(\mathbf{t}_a)\Lambda_{3,1,2} &= T(\mathbf{t}_b)\Lambda_{3,1,2} = \Lambda_{3,1,1}. \end{aligned} \tag{26}$$

We also used Eq. (22) for the spin rotations in Eq. (25). This solution is denoted by $ASDW_2$, and its spin structure is shown in Fig. 2(2). Other ASDW solutions are obtained quite similarly and their structures are shown in Figs. 2(3)–2(6).

2. $PSDW_1 \sim PSDW_4$

Now let us move to the SDW solutions whose spin directions are not collinear but coplanar. These solutions are called PSDW. For convenience, we take the xy plane for the spin directions. First, we take $\Lambda_{1,1,1} - \Lambda_{2,1,2}$ as a basis of the order parameter space Γ_7. From Eqs. (12) and (14), we obtain

$$\begin{aligned} u_{2x}\Lambda_{1,1,1} &= \Lambda_{1,1,1}, \quad C_2\Lambda_{1,1,1} = \Lambda_{1,1,1}, \\ u_{2x}\Lambda_{2,1,2} &= -\Lambda_{2,1,2}, \quad C_2\Lambda_{2,1,2} = -\Lambda_{2,1,2}. \end{aligned} \tag{27}$$

Thus, this basis is invariant to C_2u_{2x}. Furthermore, as the spin direction of this basis is perpendicular to the z axis, it is antisymmetric for the spin rotation by π around the z axis. From Eq. (13), this basis is also antisymmetric for $T(2\mathbf{t}_a)$ and $T(2\mathbf{t}_b)$ translations. Therefore, the basis is symmetric for $T(2\mathbf{t}_a)u_{2z}$ and $T(2\mathbf{t}_b)u_{2z}$. It also satisfies

$$\begin{aligned} u_{4z}^+\Lambda_{1,1,1} &\equiv u(\mathbf{e}_z,\pi/2)\Lambda_{1,1,1} = \Lambda_{2,1,1}, \\ T(\mathbf{t}_a)\Lambda_{2,1,1} &= -\Lambda_{2,1,2}, \\ u_{4z}^+\Lambda_{2,1,2} &= -\Lambda_{1,1,2}, \quad T(\mathbf{t}_a)\Lambda_{1,1,2} = \Lambda_{1,1,1}, \end{aligned} \tag{28}$$

which means the basis is invariant for $T(\mathbf{t}_a)u_{4z}^+$. The basis is also invariant for $T(-\mathbf{t}_a)u_{4z}^-$. As a result, the invariance group of Γ_7 is

$$\begin{aligned} G(\Gamma_7) = \mathbf{C}_2' L(\mathbf{t}_a - \mathbf{t}_b, 2\mathbf{t}_a + 2\mathbf{t}_b)[E + C_2u_{2x} + T(\mathbf{t}_a)u_{4z}^+ \\ + T(-\mathbf{t}_a)u_{4z}^- + T(2\mathbf{t}_a)u_{2z} + T(2\mathbf{t}_b)u_{2z}]M(\mathbf{e}_z). \end{aligned} \tag{29}$$

TABLE II. Invariance group of the SDW solutions, where $\mathbf{C}_2'$ and $\mathbf{C}_2''$ represent $\{E, C_{22'}\}$ and $\{E, C_{21'}\}$, respectively.

SDW	Invariance subgroup
$ASDW_1$	$\mathbf{D}_2 L(\mathbf{t}_a - \mathbf{t}_b, 2\mathbf{t}_a + 2\mathbf{t}_b)[E + T(2\mathbf{t}_a)u_{2x} + T(2\mathbf{t}_b)u_{2y}]A(\mathbf{e}_z)M(\mathbf{e}_y)$
$ASDW_2$	$\mathbf{C}_2' L(\mathbf{t}_a - \mathbf{t}_b, 2\mathbf{t}_a + 2\mathbf{t}_b)[E + T(2\mathbf{t}_a)u_{2x} + T(2\mathbf{t}_b)u_{2y} + T(\mathbf{t}_a)C_2 + T(\mathbf{t}_b)C_2]A(\mathbf{e}_z)M(\mathbf{e}_y)$
$ASDW_3$	$\mathbf{D}_2 L(4\mathbf{t}_a, 4\mathbf{t}_b)[E + T(2\mathbf{t}_b)u_{2y}]A(\mathbf{e}_z)M(\mathbf{e}_y)$
$ASDW_4$	$\mathbf{C}_2'' L(4\mathbf{t}_a, 4\mathbf{t}_b)[E + T(2\mathbf{t}_b)u_{2y} + T(\mathbf{t}_b)C_2]A(\mathbf{e}_z)M(\mathbf{e}_y)$
$ASDW_5$	$\mathbf{D}_6 L(4\mathbf{t}_a, 4\mathbf{t}_b)A(\mathbf{e}_z)M(\mathbf{e}_y)$
$ASDW_6$	$\mathbf{D}_3 L(4\mathbf{t}_a, 4\mathbf{t}_b)(E + C_2u_{2x})A(\mathbf{e}_z)M(\mathbf{e}_y)$
$PSDW_1$	$\mathbf{C}_2' L(\mathbf{t}_a - \mathbf{t}_b, 2\mathbf{t}_a + 2\mathbf{t}_b)(E + C_2u_{2x})[E + T(\mathbf{t}_a + \mathbf{t}_b)u_{2z} + T(2\mathbf{t}_a)u_{2z} + T(2\mathbf{t}_b)u_{2z} + T(\mathbf{t}_a)u_{4z}^- + T(-\mathbf{t}_b)u_{4z}^+]M(\mathbf{e}_z)$
$PSDW_2$	$L(4\mathbf{t}_a, 4\mathbf{t}_b)(E + C_2u_{2x})[E + C_{21'}T(\mathbf{t}_b)u_{4z}^+ + C_{21'}T(-\mathbf{t}_b)u_{4z}^- + T(\mathbf{t}_a + \mathbf{t}_b)u_{2x} + T(2\mathbf{t}_a)u_{2y} + T(2\mathbf{t}_b)u_{2z}]M(\mathbf{e}_z)$
$PSDW_3$	$\mathbf{C}_2 L(4\mathbf{t}_a, 4\mathbf{t}_b)(E + C_{22'}u_{23''})(E + C_3^+u_{3z}^+ + C_3^-u_{3z}^-)M(\mathbf{e}_z)$
$PSDW_4$	$L(4\mathbf{t}_a, 4\mathbf{t}_b)(E + C_2u_{2z})(E + C_{22'}u_{23''})(E + C_3^+u_{3z}^+ + C_3^-u_{3z}^-)M(\mathbf{e}_z)$
$CSDW_1$	$\mathbf{C}_2 L(4\mathbf{t}_a, 4\mathbf{t}_b)[T(\mathbf{t}_a + \mathbf{t}_b)u_{2x} + T(2\mathbf{t}_a)u_{2y} + T(2\mathbf{t}_b)u_{2z}](E + C_{21'}u_{2b}t)(E + C_3^+u_{31}^+ + C_3^-u_{31}^-)$
$CSDW_2$	$L(4\mathbf{t}_a, 4\mathbf{t}_b)(E + C_2t)[T(\mathbf{t}_a + \mathbf{t}_b)u_{2x} + T(2\mathbf{t}_a)u_{2y} + T(2\mathbf{t}_b)u_{2z}](E + C_{21'}u_{2b}t)(E + C_3^+u_{31}^+ + C_3^-u_{31}^-)$

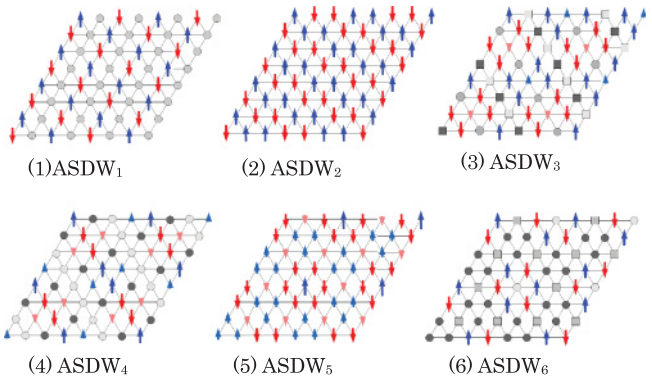

FIG. 2. (Color online) Spin structures of collinear ASDW solutions. Arrows show spin directions, and their length represents the amplitude. Circles and squares denote the sites with net charges and no spins. Different shapes and colors show different net charges.

This solution is called a PSDW$_1$. Other PSDW solutions are obtained similarly. The spin structures of all the PSDW solutions are shown in Fig. 3.

3. *CSDW$_1$ and CSDW$_2$*

We introduce the SDW solutions whose spin directions are 3D. In this paper we call them cubic-type SDW (CSDW). First let us take $\Lambda_{1,1,1}+\Lambda_{2,2,1}+\Lambda_{3,3,1}$ as the basis of the order parameter space Γ_{11}. This basis is symmetric for C_2 rotation. Furthermore, as this basis satisfies

$$\begin{aligned} &T(2\mathbf{t}_a)\Lambda_{1,1,1}=-\Lambda_{1,1,1}, \quad T(2\mathbf{t}_b)\Lambda_{1,1,1}=-\Lambda_{1,1,1},\\ &T(2\mathbf{t}_a)\Lambda_{2,2,1}=\Lambda_{2,2,1}, \quad T(2\mathbf{t}_b)\Lambda_{2,2,1}=-\Lambda_{2,2,1},\\ &T(2\mathbf{t}_a)\Lambda_{3,3,1}=-\Lambda_{3,3,1}, \quad T(2\mathbf{t}_b)\Lambda_{3,3,1}=\Lambda_{3,3,1}, \end{aligned} \tag{30}$$

it is invariant for $T(2\mathbf{t}_a)u_{2y}$, $T(2\mathbf{t}_b)u_{2z}$, and $T(2\mathbf{t}_a+2\mathbf{t}_b)u_{2x}$. In addition, from Eqs. (12) and (14), we obtain

$$\begin{aligned} &u_{2b}\Lambda_{1,1,1}=-\Lambda_{2,1,1}, \quad C_{21'}\Lambda_{2,1,1}=\Lambda_{2,2,1},\\ &u_{2b}\Lambda_{2,2,1}=-\Lambda_{1,2,1}, \quad C_{21'}\Lambda_{1,2,1}=\Lambda_{1,1,1},\\ &u_{2b}\Lambda_{3,3,1}=-\Lambda_{3,3,1}, \quad C_{21'}\Lambda_{3,3,1}=\Lambda_{3,3,1}. \end{aligned} \tag{31}$$

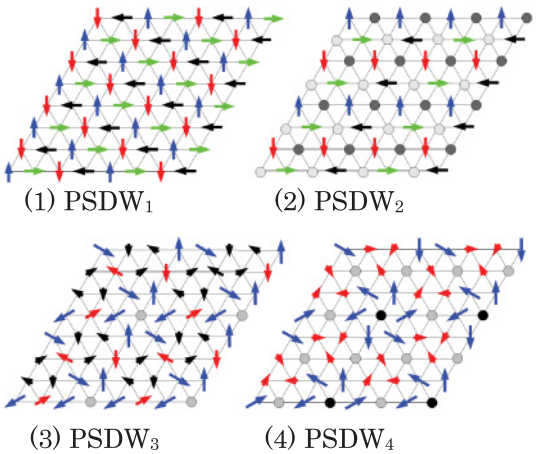

FIG. 3. (Color online) Spin structures of coplanar PSDW solutions. Notations are almost the same as in Fig. 3, but in (3) and (4), different colors, as well as their lengths, show different amplitudes.

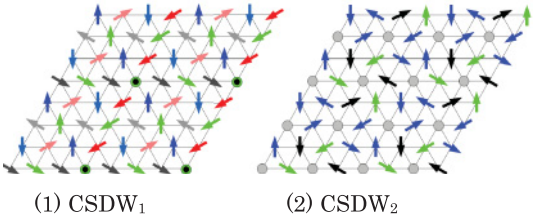

FIG. 4. (Color online) Spin structures of CSDW solutions. In (1), the view is seen from (1,1,1) direction. Red, gray, and blue arrows represent the positive directions of the x, y, and z axes, respectively, while the corresponding light colors represent their negative directions. Circles represent the spin perpendicular to the paper [(1,1,1)-direction]. In (2), black, green, and blue arrows represent the spin directions, upward, downward, and parallel to the paper, respectively. Circles denote the sites with no net spins.

Thus, this basis is invariant for $C_{21'}u_{2b}t$. Finally, we point out an interesting symmetry characteristic of 3D spin alignment. We consider the spin rotation by $2\pi/3$ around $x=y=z$, which is denoted by u_{31}^{+}. From Eqs. (12) and (14), we obtain

$$\begin{aligned} &u_{31}^{+}\Lambda_{1,1,1}=\Lambda_{2,1,1}, \quad C_3^{+}\Lambda_{2,1,1}=\Lambda_{2,2,1},\\ &u_{31}^{+}\Lambda_{2,2,1}=\Lambda_{3,2,1}, \quad C_3^{+}\Lambda_{3,2,1}=\Lambda_{3,3,1},\\ &u_{31}^{+}\Lambda_{3,3,1}=\Lambda_{1,3,1}, \quad C_3^{+}\Lambda_{1,3,1}=\Lambda_{1,1,1}, \end{aligned} \tag{32}$$

which means this basis is invariant for $C_3^{+}u_{31}^{+}$. Thus, the invariant group of this order parameter space is

$$\begin{aligned} G(\Gamma_{11})=\mathbf{C}_2L(4\mathbf{t}_a,4\mathbf{t}_b)[&E+T(2\mathbf{t}_a+2\mathbf{t}_b)u_{2x}+T(2\mathbf{t}_a)u_{2y}\\ &+T(2\mathbf{t}_b)u_{2z}](E+C_{21'}u_{2b}t)(E+C_3^{+}u_{31}^{+}+C_3^{-}u_{31}^{-}). \end{aligned} \tag{33}$$

Another CSDW solution is also classified in the similar way. Spin structures of these CSDW solutions are shown in Fig. 4.

Among these UHF solutions, ASDW$_2$ shown in Fig. 2(2) becomes the HF ground state in the weak and intermediate interaction regimes. We show in Fig. 5 the U dependence of the UHF energies for ASDW$_2$ and 120° AF states. In the strong interaction regimes, the lowest UHF state is 120° AF state, which is qualitatively consistent with the previous researches.[8–10] In the following, we focus on the electronic structures in the weak interaction regime ($U/t=4.5$–5).

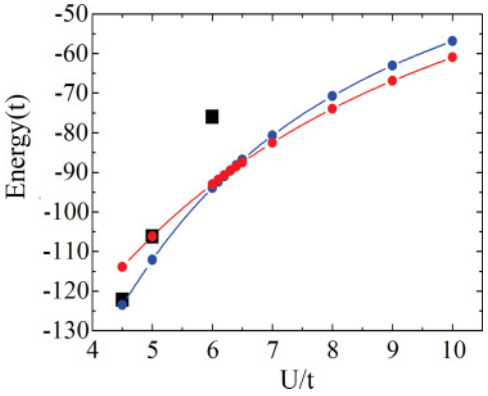

FIG. 5. (Color online) U/t dependence of the energies for ASDW$_1$ (black squares), ASDW$_2$ (blue circles), and 120° AF (red circles) states. Solid lines are guides for the eyes.

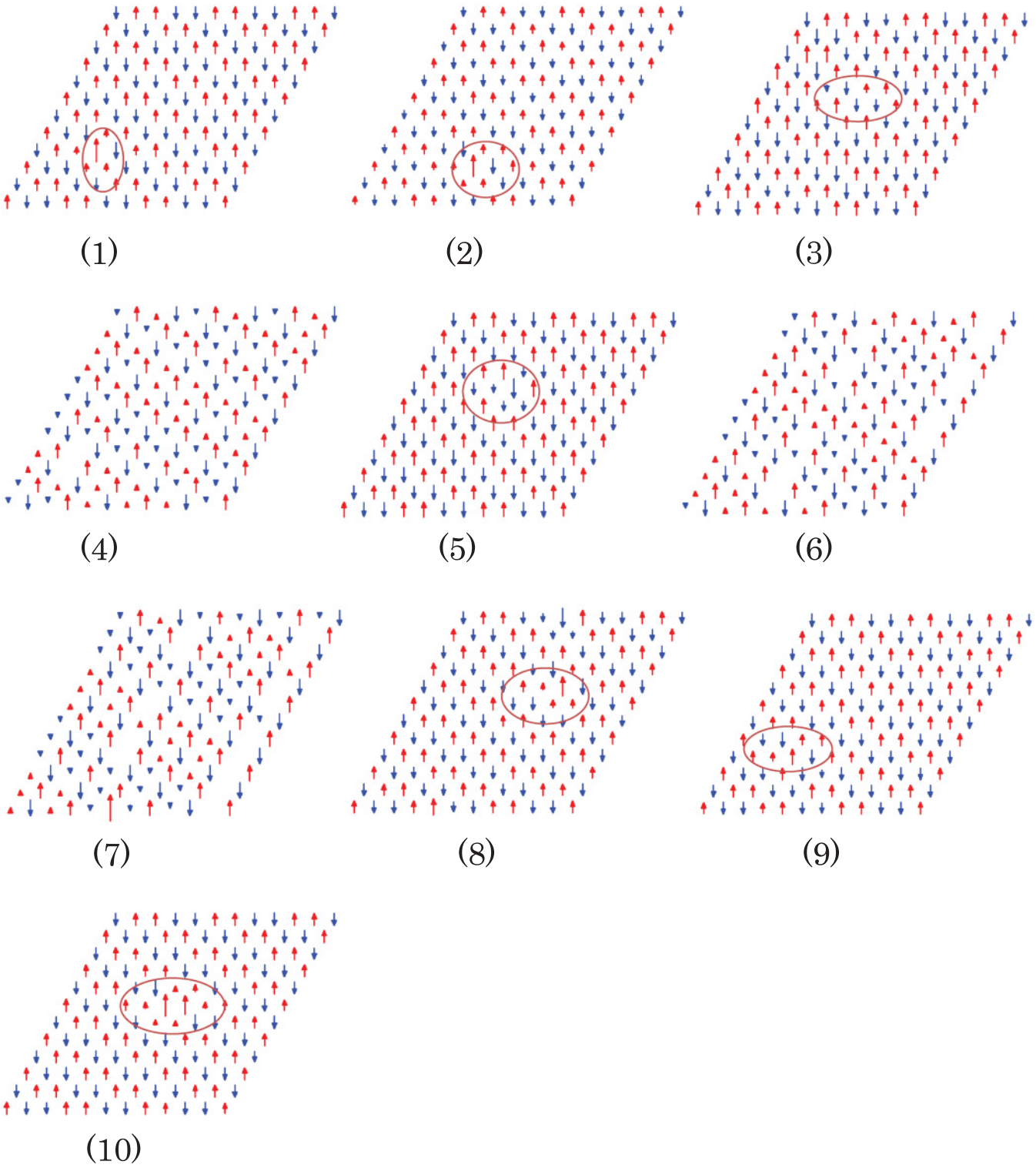

FIG. 6. (Color online) Spin structures of $N_S = 10$ Slater determinants generating the resonating HF wave functions for $U/t = 4.5$.

B. Resonating HF calculations

For further investigation to incorporate the electron correlation effects, we apply the resonating HF method to this frustrated system. In the following, the system size is $N = 12 \times 12$, and we superpose $N_S = 10$ Slater determinants [and their symmetry adopted ones denoted by P^G in Eq. (2)] to construct a many-body wave function. The group theoretical classification for the UHF solutions is useful for the resonating HF study since it gives important information on trial Slater determinants to be superposed. Specifically, the lowest UHF solution in the weak interaction regime ($U \sim 4.5$) is the ASDW_2 and, therefore, we employ this ASDW_2 and its

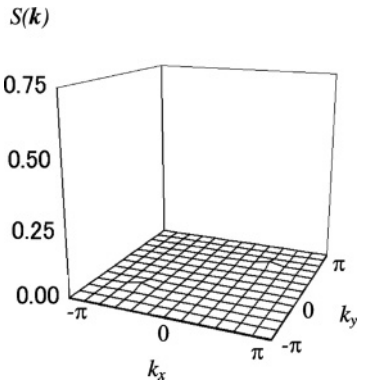

FIG. 7. Spin correlation function $S(\mathbf{k})$ for $U/t = 4.5$.

low-energy excited states as initial Slater determinants. On the other hand, in Fig. 6, we show all the optimized Slater determinants generating the resonating HF wave function for $U/t = 4.5$. In this figure, the up and down spins are denoted by the red and blue arrows, respectively, and the spin amplitude is represented by length of the arrow. We can see the spin flipping or modulation from the uniform $ASDW_2$ ordering in Figs. 6(1)–6(3), 6(5), and 6(8)–6(10). Areas where the spin modulations are significant are marked by ovals. One of the most important features is that we obtain the Slater determinants whose spin structures are very close to the $ASDW_1$, as shown in Figs. 6(4), 6(6), and 6(7). In fact, we did not take such configurations as the initial Slater determinants, and the orbital optimization worked to incorporate the electron correlation effects efficiently. From Fig. 6, we can say that quantum fluctuations are described by quantum interference among the $ASDW_1$-like states and $ASDW_2$-like states as well as their symmetry adopted ones.

Now we can speculate that quantum fluctuations due to such hybridization of Slater determinants having different spin structures and spin modulations will reduce the LRO of the spin correlation. In Fig. 7, we show the spin correlation functions calculated from the resonating HF wave function. Here we define $S(\mathbf{k})$ as

$$S(\mathbf{k}) = \frac{1}{N}\sum_{i,j}\langle \mathbf{S}_i \cdot \mathbf{S}_j\rangle e^{-i\mathbf{k}\cdot\mathbf{r}_{ij}}, \tag{34}$$

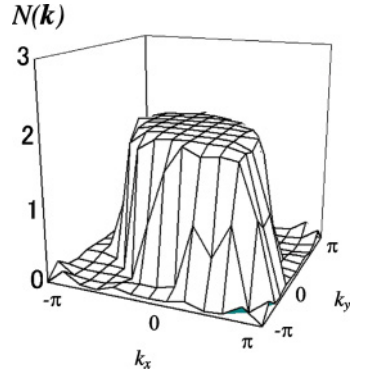

FIG. 8. (Color online) Momentum distribution of electron density $N(\mathbf{k})$ for $U/t = 4.5$.

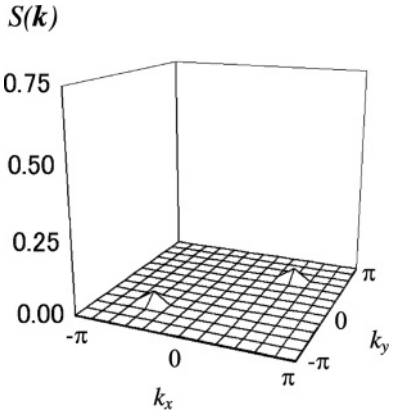

FIG. 9. $S(\mathbf{k})$ for $U/t = 5$.

where $\mathbf{r}_{ij}$ denotes the relative coordinate between the sites i and j. This and the following momentum dependences are calculated by transforming the original triangular lattice to the topologically equivalent square lattice with diagonal transfers.[9,10] We cannot see any significant structures except small ones at $\mathbf{k} = (\pi/2,\pi/2)$ and $(-\pi/2, -\pi/2)$, which would reflect the $ASDW_2$-like spin configuration. This structure is as small as 1.4×10^{-2}, and therefore, the present result is consistent with the previous ones, which conclude that no LRO exists in this interaction regime.[9,10] However, as shown above, our results give more explicit spin structures through the Slater determinants generating the resonating HF wave function. We should emphasize that this spin structure is not simply paramagnetic but the spin correlation is eliminated by large quantum fluctuations due to hybridization of Slater determinants having different spin structures and spin modulations.

Here we define $N(k)$ as

$$N(\mathbf{k}) = \sum_{i,j,\sigma}\langle a^{\dagger}_{i\sigma} a_{j\sigma}\rangle e^{-i\mathbf{k}\mathbf{r}_{ij}}. \tag{35}$$

This represents the momentum distribution of electrons, and therefore, it should have jumps at the Fermi wave numbers when the system is metallic. In fact, as shown in Fig. 8, $N(\mathbf{k})$ for $U/t = 4.5$ has clear jumps, which indicates the system is metallic. It is interesting that each Slater determinant generating the resonating HF wave function is close to the

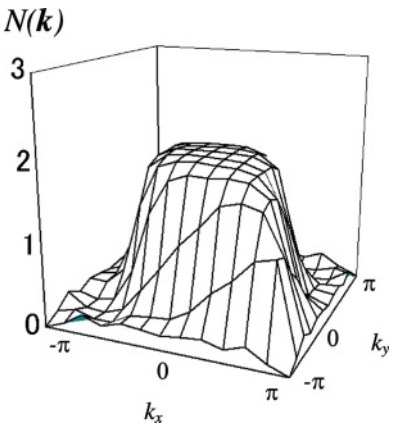

FIG. 10. (Color online) $N(\mathbf{k})$ for $U/t = 5$.

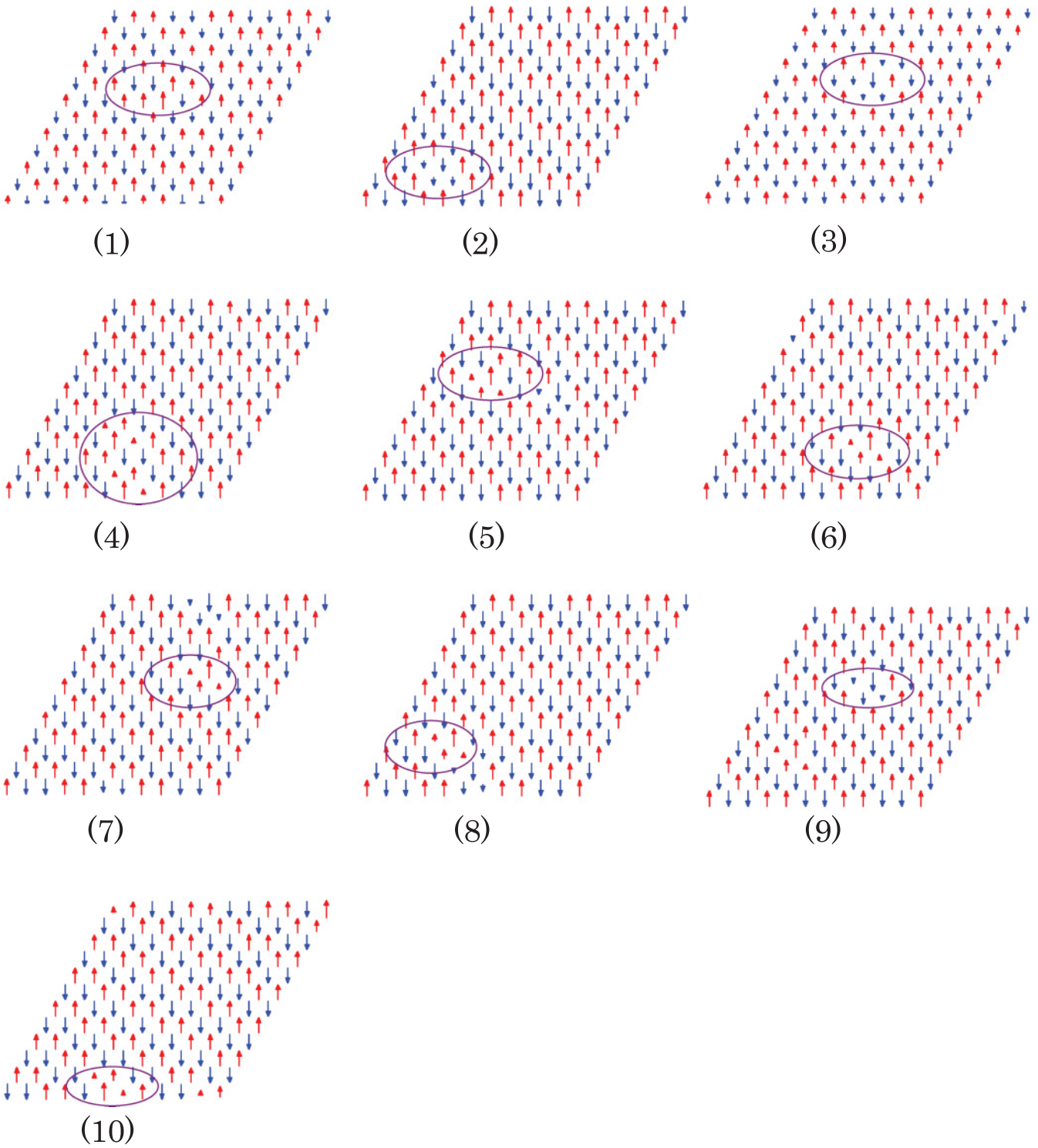

FIG. 11. (Color online) Structures of $N_S = 10$ Slater determinants generating the resonating HF wave functions for $U/t = 5$.

ASDW_1 or ASDW_2 configurations, but the total wave function shows the metallic behavior. This would be also caused by the quantum fluctuations.

Next, we show $S(\mathbf{k})$ and $N(\mathbf{k})$ for $U/t = 5$ in Figs. 9 and 10, respectively. We can see that the spin structure is slightly increased ($\sim 4.5 \times 10^{-2}$) and the slope in $N(\mathbf{k})$ becomes gentle, though the system seems still nonmagnetic and metallic, as in the case of $U/t = 4.5$. We can find the reason for this change in the electronic structures into the change in the character of quantum fluctuations. In Fig. 11, we show the spin structures of the Slater determinants generating the resonating HF wave function for $U/t = 5$. We cannot find Slater determinants having the ASDW_1-like spin structure. The reason is as follows. The energy of the ASDW_1 solution

largely increases as the increase of U/t, compared to $ASDW_2$ solution, as shown in Fig. 5. In the case of $U/t = 4.5$, the energy of the $ASDW_1$ is very close to that of the $ASDW_2$, and therefore, the resonance of these two states can effectively work to lower the ground-state energy. However, when U/t is increased, the energy of the $ASDW_1$ becomes much higher than that of the $ASDW_2$, and the resonance with the $ASDW_1$ does no work to lower the ground-state energy. Thus, the change in electronic structures is reasonably described by the quantum fluctuations.

Our purpose is not to lower the ground-state energy as much as possible but to obtain physics for the complicated spin structures in the frustrated systems. Therefore, as shown above, $N_S = 10$ Slater determinants are enough. Here, for the future works, we just mark the ground-state energy of the resonating HF wave function at $U/t = 4.5$, that is $-132.7t$ for the $N = 12 \times 12$ system. We are also interested in the metal-insulator transition or competition between the nonmagnetic insulating and 120° AF states in the intermediate and strong interaction regimes. PIRG calculations for $N = 6 \times 6$ predicted a very complicated phase diagram there. Quantum fluctuations in these interaction regimes will be investigated elsewhere in the near future.

Finally, we briefly mention the finite-size effect. It is difficult to exactly determine whether the system has a real LRO or not in the thermodynamic limit, even though the spin correlation is extremely small in our finite-size calculations. In the thermodynamic limit, simple overlap between the UHF solutions, for example, $ASDW_1$ and $ASDW_2$, would be 0. However, the optimized Slater determinants generating the resonating HF state have significant modulations from the uniform UHF states, as shown in Figs. 6 and 11. Such modulations are important to make resonance between $ASDW_1$-like and $ASDW_2$-like states finite in the thermodynamic limit. In addition, hybridization of the $ASDW_1$ and $ASDW_2$ can contribute to physics, through the Slater determinants which are nonorthogonal to both of these two states, even if their direct overlap goes to zero. Thus, we think the resonating HF picture, mentioned above, would hold in the thermodynamic limit, though numerical research is restricted to finite size systems. A scaling analysis will be done in the near future.

IV. SUMMARY

We have clarified the detailed electronic structures of the Hubbard model on the uniform triangular lattice in the weak interaction regime. First, we have classified the UHF solutions according to the group theory. Then, by using information obtained from the group theoretical classification, the resonating HF calculations have been carried out. We have shown that the system is metallic and nonmagnetic in the weak interaction regimes. This is not a simple paramagnetism but spin correlation is eliminated (or significantly reduced) by large quantum fluctuations due to hybridization of Slater determinants having different spin structures and spin modulations. Thus, we have obtained the physics behind the electron correlations in terms of the quantum fluctuations.

ACKNOWLEDGMENTS

This work was partially supported by Grand-in-Aid for Scientific Research No. 23540359 and the Next Super Computing Project, Nanoscience Program, MEXT, Japan.

[1] H. Urayama, H. Yamochi, G. Saito, K. Nozawa, T. Sugano, M. Kinoshita, S. Sato, K. Oshima, A. Kawamoto, and J. Tanaka, Chem. Lett. **1988**, 55 (1988).
[2] K. Kanoda, Physica C **282-287**, 299 (1997).
[3] A. P. Ramirez, in *Handbook of Magnetic Materials*, edited by K. J. H. Buschow (Elsevier Science, Amsterdam, 2001).
[4] Y. Shimizu, K. Miyagawa, K. Kanoda, M. Maesato, and G. Saito, Phys. Rev. Lett. **91**, 107001 (2003).
[5] H. Kino and H. Fukuyama, J. Phys. Soc. Jpn. **65**, 2158 (1996).
[6] H. Kondo and T. Moriya, J. Phys. Soc. Jpn. **68**, 3170 (1999).
[7] J. Merino and R. H. McKenzie, Phys. Rev. Lett. **87**, 237002 (2001).
[8] F. Mezzacapo and J. I Cirac, New. J. Phys. **12**, 103039 (2010).
[9] H. Morita, S. Watanabe, and M. Imada, J. Phys. Soc. Jpn. **71**, 2109 (2002).
[10] T. Yoshioka, A. Koga, and N. Kawakami, Phys. Rev. Lett. **103**, 036401 (2009).
[11] L. Capriotti, A. E. Trumper, and S. Sorella, Phys. Rev. Lett. **82**, 3899 (1999).
[12] D. A. Huse and V. Elser, Phys. Rev. Lett. **60**, 2531 (1988).
[13] H. Fukutome, Prog. Theor. Phys. **80**, 417 (1988).
[14] N. Tomita, Phys. Rev. B **69**, 045110 (2004).
[15] N. Tomita and S. Watanabe, Phys. Rev. Lett. **103**, 116401 (2009).
[16] H. Fukutome, Prog. Theor. Phys. **52**, 115 (1974).
[17] M. Ozaki and H. Fukutome, Prog. Theor. Phys. **60**, 1322 (1978).
[18] M. Ozaki, J. Math. Phys. **26**, 1514 (1985).
[19] M. Golubitsky, I. Stewart, and D. G. Schaeffer, *Singularities and Groups in Bifurcation Theory II* (Springer-Verlag, Berlin, 1985).
[20] A. Nakanishi, M. Hamada, A. Goto, and M. Ozaki, Prog. Theor. Phys. **118**, 413 (2007).
[21] A. Ikawa and M. Ozaki, J. Phys. Condens. Matter **4**, 4039 (1992).